Solving the advection-diffusion equations in biological contexts using the cellular Potts model

Debasis Dan,* Chris Mueller, Kun Chen, and James A. Glazier†
Biocomplexity Institute and Department of Physics, Indiana University, 727 E. 3rd Street, Swain Hall West 159, Bloomington, Indiana 47405-7105, USA
(Received 26 April 2005; published 10 October 2005)

The cellular Potts model (CPM) is a robust, cell-level methodology for simulation of biological tissues and morphogenesis. Both tissue physiology and morphogenesis depend on diffusion of chemical morphogens in the extra-cellular fluid or matrix (ECM). Standard diffusion solvers applied to the cellular potts model use finite difference methods on the underlying CPM lattice. However, these methods produce a diffusing field tied to the underlying lattice, which is inaccurate in many biological situations in which cell or ECM movement causes advection rapid compared to diffusion. Finite difference schemes suffer numerical instabilities solving the resulting advection-diffusion equations. To circumvent these problems we simulate advection diffusion within the framework of the CPM using off-lattice finite-difference methods. We define a set of generalized fluid particles which detach advection and diffusion from the lattice. Diffusion occurs between neighboring fluid particles by local averaging rules which approximate the Laplacian. Directed spin flips in the CPM handle the advective movement of the fluid particles. A constraint on relative velocities in the fluid explicitly accounts for fluid viscosity. We use the CPM to solve various diffusion examples including multiple instantaneous sources, continuous sources, moving sources, and different boundary geometries and conditions to validate our approximation against analytical and established numerical solutions. We also verify the CPM results for Poiseuille flow and Taylor-Aris dispersion.

DOI: 10.1103/PhysRevE.72.041909 PACS number(s): 87.10.+e, 02.70.Uu, 05.10.−a, 47.11.+j

I. INTRODUCTION

Advection-diffusion equations (ADE) describe a broad range of natural phenomena. They occur in diverse fields including physics [1], chemistry [2], biology, geology [3,4], and even in migration and epidemiology [5]. They describe the flow (deterministic) and the spread (stochastic) of a density (of a chemical, heat, charge) which a fluid or deformable solid carries. The simplest ADE is

$$\frac{\partial n}{\partial t} = D\nabla^2 n - \vec{v}\cdot\vec{\nabla} n, \tag{1}$$

where n is the density of the transported substance, D its diffusion constant (here assumed uniform in space), and $\vec{v}$ is the velocity field. The velocity field in turn couples to the pressure field of the medium through the Navier-Stokes equations. Though we can solve the problem analytically in steady state with simple boundary conditions, most physically relevant ADEs appear within sets of nonlinear coupled equations or with nontrivial boundary conditions where analytical solutions are not possible [6]. Hence a vast literature exists on how to solve ADEs. Most solvers use either finite difference (FD) or finite element (FE) [7] schemes. Besides these deterministic approaches, several schemes use Lattice-Boltzmann (LB) methods [8] like Flekkoy's method [9], Dawson's method, [10], and the moment-propagation method [11]. ADEs in general are difficult to solve in the absence of separation of diffusion and advection time scales or in the presence of moving boundaries. Most lattice-based methods locally refine the grid during solution to avoid instabilities. Moreover, explicit LB methods require time averaging of the torque to avoid instabilities [12]. Hence the computational cost of both LB and deterministic methods shoots up. Nonstaggered FD grids may show grid-decoupling instabilities [12]. Also, all explicit methods require consideration of the general stability constraints from linear analysis, most notably the Neumann diffusive criterion linking the time step and the square of the grid size. In this paper we try to address the problems associated with incorporating advection diffusion in biologically motivated, multiscale simulations, specifically those which use the cellular Potts model (CPM) to model cell behaviors.

Diffusion of morphogens and flow of extra-cellular matrix (ECM) are crucial to many biological phenomena, including wound healing, morphogenesis, e.g., during mesenchymal condensation or gastrulation [13] and the immune response where cells emerge from the microvasculature and migrate toward sites of inflammation to kill bacteria, other pathogens, and cancer. The generic mechanisms common to all these processes are changes in cell velocities (*chemotaxis*) or/and differentiation in response to the temporal and spatial variations of chemical morphogens. Other classic examples of diffusion-driven morphogenesis involve Turing instabilities. Turing instabilities arise due to different diffusion rates of two or more reacting chemicals resulting in competition between activation by a slow-diffusing chemical (*activator*) and inhibition by a faster chemical (*inhibitor*). Pattern formation during morphogenesis due to Turing instabilities is a subject by itself [14].

Besides chemotaxis, the formation and rate of extension of pseudopods which crucially depends on convective mass transport [15,16] also influences cell motility. Hydrodynamic shear can also increase cell-cell adhesion efficiency by in-

*Electronic address: ddan@indiana.edu
†Electronic address: glazier@indiana.edu

creasing the number of binding receptors. Shear has a profound effect on neutrophil-platelet adhesion and neutrophil aggregation, key events in acute coronary syndromes like arterial thrombosis ([17]). Extensive work has shown that both fluid shear amplitude and shear exposure time modulate the interactions between polymorphonuclear leukocytes and colon carcinoma cells [18]. Gene expression and protein synthesis in endothelial cells also change upon application of arterial shear stresses [19]. In a prominent example, fluid shear allows optimal L-selectin-mediated leukocyte rolling only above a minimum threshold shear rate [20]. Hence multicellular modeling tools have to properly account for the advection-diffusion: Diffusion influencing the spatial and temporal distribution of chemical morphogens, advection controlling the rates of cell collisions, deformation, receptor-ligand bond formation [21], adhesion, and enhanced mixing of chemical morphogens.

Simulations of the development of multicellular organisms take diverse mathematical approaches: continuum FE-based models [22] of reaction diffusion which consider cell density as a continuous variable [23], hybrid models like E-cell [24] and cellular automaton approaches [25]. Glazier and Graner developed the cell-level CPM, an extension of the energy-based large-Q Potts model, for organogenesis simulations [26]. The basic CPM explains how surface binding energies drive cell movement and models cell sorting from an initial random distribution into different patterns depending on the cell adhesion coefficients at homotypic, heterotypic, and cell-medium boundaries [27]. It also provides a platform on which to build simulations of a wide range of biological experiments by including additional mechanisms like directed active movement due to external fields, e.g., chemotaxis to a chemical field gradient, gravity, or cell polarity. CPM applications include modeling mesenchymal condensation [25,28,29], the complete life-cycle of *Dictyostelium discoideum* [30], tumor growth [31], vascular development [32], immune response, and limb growth [33]. Unlike the simple Turing mechanism where cells have no feedback on the chemical field, most CPM implementations include this feedback which can give rise to completely different patterning from the Turing mechanism. In the CPM, patterns can arise under the influence of a single chemical field [13] due to cell movement, biased by gradients in cell-cell adhesion and cell-ECM binding, which is impossible in Turing mechanism. This unique mechanism also differs from chemotaxis, which requires long-range cell movement [28].

All existing CPM implementations suffer from four main limitations: (1) They do not include viscous dissipation explicitly. Instead dissipation arises from the Metropolis-Boltzmann energy-minimization dynamics. This implicit dissipation makes viscosity hard to calculate or control. (2) They do not explicitly describe force transduction through cells, which arises through the volume constraint and surface constraint (if used) of the Hamiltonian. (3) Aggregates of cells modeled with an ordinary CPM Hamiltonian are highly overdamped. Modeling the ECM or fluid as an array of generalized cells using the normal CPM produces a flow resembling the overdamped flow of biological fluid but this fluid slips at solid surfaces and exerts no shear force unlike a normal fluid. An alternative approach which describes the fluid as a single, large, unconstrained generalized cell produces nonlocal movement. Moreover, it cannot advect chemicals or transmit shear forces. (4) The CPM has no intrinsic concept of rigid-body motion. We will describe an algorithmic solution to this last problem, which makes the CPM look more like a FE simulation, in a future paper.

All of these problems result from the CPM spins being tied to the underlying lattice, rather than to objects they describe. The solution in each case is to adopt a FE approach suited to the CPM, which takes the behavior off lattice. Applying standard off-lattice methods in the CPM has inherent problems. Since in the CPM cell movement occurs by boundary fluctuations, connecting normal FE fluid solvers to the CPM at surfaces requires local grid refinement during cell movement to avoid numerical instabilities. Hence its computational cost is high.

To introduce advection diffusion in the CPM correctly and efficiently, we propose an off-lattice scheme consistent and in harmony with the CPM algorithm. We subdivide the ECM into small fluid particles having the normal properties of generalized cells like differential adhesivity, a surface constraint and a volume constraint. The fluid particles carry chemical morphogens and we assume the concentrations are uniform inside them. Diffusion occurs between neighboring fluid particles by local averaging rules which approximate the Laplacian. Spin flips in the CPM occur only at the boundaries of the cells or particles. A force on the fluid in any direction due to pressure gradients or external forces biases the probability of spin flips and generates directed motion [34]. We introduce viscosity into the CPM by explicitly including in the Hamiltonian including a relative-velocity constraint between the neighboring fluid particles. This scheme allows us to solve the ADEs and generates the creeping flow of a highly viscous fluid.

In most biologically relevant regimes (e.g., *E. Coli* in water), we encounter low Reynolds number (Re) flow $\sim 10^{-5}$, with the typical diffusion coefficient of chemical morphogens being $\sim 10^{-4}$ $\mu m^2/s$. Thus the Peclet number (defined as Rv/D, where R, v, D are typical size of the system, the typical fluid velocity, and diffusion coefficient, respectively) is as low as $\sim 10^{-2}$ [35]. We explicitly exclude blood flow in the circulatory system, where Re numbers (hence inertia) can be quite large and where specialized solution techniques already exist. Since most CPM simulations do not demand high precision, sophisticated methods like mimetic finite difference [36] become a computational bottleneck without many advantages. On the other hand, our ADE scheme is very stable, with spatial resolution equal to the mean diameter of the fluid particles, which are much smaller than the simulated biological cells. Our scheme seamlessly integrates into the main Monte Carlo loop of the CPM simulation and boundary conditions like absorbing boundaries or no-flux boundaries are simple to implement. More-over our off-lattice scheme does not require remeshing. We discuss these issues in detail below.

This paper mainly focuses on the validity and utility of the CPM ADE solver. Section II briefly describes the CPM along with the diffusion and advection scheme. Section III discusses various cases, including diffusion from two point sources, a continuous source, and a moving source with ei-

ther reflecting or absorbing boundary conditions and the flow profile in Poisueille's flow. Section IV outlines future directions in developing the ADE scheme. We will address in a future paper certain additional conditions, flow with inertia, effects of low or high Peclet numbers, constitutive properties of the fluid phase, etc. As we have stated before, ours method provides flexibility and efficiency in the biologically relevant regime of low Peclet and Reynolds numbers and where high numerical accuracy is not crucial.

II. MODEL

The Potts model is an energy-based, lattice cellular-automaton (CA) model equivalent to an Ising model with more than two degenerate spin values. We typically use a cubic lattice with periodic or fixed boundary conditions in each direction. We use third or fourth nearest neighbor interactions to reduce lattice-anisotropy induced alignment and pinning. Each lattice site in the Potts model has a spin value. The energy, or *Hamiltonian* sums the interaction energies of these spins, according to predefined rules. In single-spin dynamics (like Metropolis dynamics) the spin lattice evolves toward its equilibrium state by minimizing the interaction energy through spin flips. Multispin dynamics like Kawasaki dynamics are also possible. Though the original Potts model studies focuses on equilibrium properties, it can also model quasiequilibrium dynamical properties [37]. Using deterministic schemes for spin flips, patterns often stick in local minima. Finite-temperature Monte Carlo schemes circumvent this problem. These schemes accept a spin flip with temperature dependent Boltzmann or modified Boltzmann probability if the configuration encounters a potential barrier (a greater energy after the spin flip than before) [37].

We pick a target lattice site at random and one of its alien neighbors, also selected at random and attempt to flip the target spin to the value of the selected neighbor. In the modified Metropolis algorithm we employ, if the spin flip would produce a change in energy ΔH, we accept the change with probability P given by

$$P(\Delta H) = \begin{cases} \exp(-\Delta H/T) & \text{if } \Delta H > 0, \\ 1 & \text{otherwise}, \end{cases} \tag{2}$$

where T is the fluctuation temperature. T controls the rate of acceptance of the proposed move. For very large T, all the moves are accepted and the dynamics is a random walk in the absence of barriers, i.e., interaction energies included in the Hamiltonian are effectively zero producing a disordered phase. For very small values of T the dynamics is deterministic and can trap in local minima. We choose T as the median value of the distribution of ΔH, which is below the order-disorder phase transition temperature. All of our results are very robust with respect to a variation of T. S. Wong has recently shown that optimizing the dynamics of the modified Metropolis algorithm requires changes to the acceptance probability in Eq. (2) [38]. However, we do not implement these changes here. Our unit of time is Monte Carlo sweep (MCS), where $1\text{MCS}=L^3$ spin flip attempts, L being the system size.

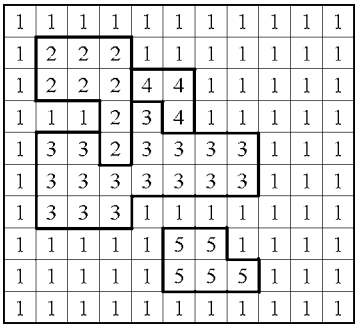

FIG. 1. A typical cell configuration in CPM. The bold lines denote cell boundary.

The CPM adapts the Potts model to the context of biology. A CPM cell is a collection of lattice sites with same spin value (or index) σ_i. Each cell has a unique spin σ (see Fig. 1). Cells may also have additional characteristics, e.g., a type τ. Links between different sites with spins define cell boundaries. So cells have both volume and a surface area. The volume, area, and radius relations are highly non-Euclidean for small cells.

The CPM Hamiltonian contains a variable number of terms. The interaction between pairs of biological cells involves an adhesive or repulsive interfacial energy. This interfacial energy is precisely the Potts energy, the sum of the interactions of neighboring unlike spins, across a link. Each mismatched link contributes a cell-type dependent binding energy per unit area $J(\tau,\tau')$, where τ and τ' are the type of cells on either side of the link. In the CPM the effective cell-cell interaction energy is

$$E_{\text{adhesion}} = \sum_{(i,j,k),(l,m,n)\text{neighbors}} J[\tau_{\sigma(i,j,k)}, \tau_{\sigma(l,m,n)}] \times \{1 - \delta_{[\sigma(i,j,k),\sigma(l,m,n)]}\}, \tag{3}$$

where $\delta_{(\sigma',\sigma)}=1$ if $\sigma'=\sigma$, otherwise $\delta_{(\sigma',\sigma)}=0$.

At any time t, a cell, of type τ has a volume $v(\sigma,t)$ and surface area $s(\sigma,t)$. The volume is simple to define, $v(\sigma_0) = \Sigma_{i,j,k}\delta_{[\sigma_0,\sigma(i,j,k)]}$, whereas surface area is more complex, since it depends on the interaction range of the lattice, $s(\sigma_0)=\Sigma_{i,j,k}\delta_{(\sigma_0,\sigma_{i,j,k})}\Sigma_{i',j',k'}\{1-\delta_{[\sigma(i,j,k),\sigma(i',j',k')]}\}$, where (i,j,k) and (i',j',k') are neighboring lattice sites. Each cell has an effective volume elasticity, λ_v and target volume $v_{\text{target}}(\sigma,t)$. Larger values of λ_v, produce less compressible cells. We typically choose $v_{\text{target}}^2\lambda_v >$ other constraint energies. This compressibility makes little difference in low Reynolds number flow but makes pattern evolution less stiff. We also define a membrane elasticity λ_s and a target surface area $s_{\text{target}}(\sigma,t)$ to maintain the generalized shape of the cells. The energy contributions due to surface and volume fluctuations are

$$E_{\text{surface}} = \lambda_s[s(\sigma,t) - s_{\text{target}}(\sigma,t)]^2, \tag{4}$$

$$E_{\text{volume}} = \lambda_v[v(\sigma,t) - v_{\text{target}}(\sigma,t)]^2. \tag{5}$$

We can extend the Hamiltonian to include a uniform external force $\vec{F}$, acting on all cells by including the term

$$E_{\text{force}} = -\sum_{(ijk),(lmn)\text{neighbors}} \vec{\mathbf{F}} \cdot \vec{\mathbf{r}}_{i,j,k}[1 - \delta_{\sigma(i,j,k),\sigma(l,m,n)}], \quad (6)$$

where $\vec{\mathbf{r}}_{ijk}$ is the position vector at the lattice site (i,j,k).

Previous CPM applications often treated fluid or ECM as a single large cell with no constraints. Here we take the coarse-grained approach to describe ECM. We assume the ECM consists of hypothetical fluid cells (which we call particles to avoid confusion with the modeling of biological cells) having all the characteristic interactions and constraints of regular CPM cells. The volume constraint and the surface tension determine the elastic nature of the fluid. The fluid particles can move with respect to one another like a regular CPM cell via spin flips. Thus, local pressure developed due to movement or enlargement of actual biological cells will translate into motion of the surrounding ECM. This fluid motion causes advection and mixing along with molecular diffusion of chemical morphogens. We restrict consideration to the highly overdamped viscous world that most biological cells experience, so our fluid particles lack inertia. We also restrict to situations where the velocity of movement is much less than the velocity of sound, which is one lattice unit per MCS.

We now introduce a relative velocity constraint between the cells/particles which faithfully captures the effects of shear due to the viscosity of the medium. In the CPM, velocity is a cell property defined as the displacement of the center of mass of the cell per MCS. Since the velocity gradient terms in the direction of the flow (e.g., $\partial u_i/\partial x_i$) are the rate of change of volume [40] which Eq. (5) already includes, we need to keep only the contributions of cross terms of the form $(\partial u_i/\partial x_j)^2$. In an incompressible fluid ($\boldsymbol{\nabla}\cdot\mathbf{u}=0$) the cross terms are the dissipation energy per unit volume [6]. In the CPM we model this term as

$$E_{\text{viscosity}} = \lambda_{\text{viscosity}} \sum_i \sum_j S_{ij} \frac{(V_{i_x} - V_{j_x})^2}{d_{ij}^2} \sqrt{\frac{(y_i - y_j)^2 + (z_i - z_j)^2}{d_{ij}^2}} + \text{cyclic permutation of } (x,y,z), \quad (7)$$

where the j's are the indices of cells neighboring the ith cell and $d_{ij} = \sqrt{(x_i - x_j)^2 + (y_i - y_j)^2 + (z_i - z_j)^2}$ is the distance between the centers of cell i and cell j. V_{i_x} is the $\hat{x}$-component of the velocity of the ith cell. Since the cells are of irregular shape, we further weight the energy penalty by the cells common contact area S_{ij}. We ensure that the cells are simply connected by using local connectivity checks during spin flip attempts. $\lambda_{\text{viscosity}}$ corresponds to the viscosity coefficient η in the Navier-Stokes equations. η has dependence on other system parameters like J, λ_{volume}, and λ_{surface}.

The net Hamiltonian including fluids is then

$$H = E_{\text{adhesion}} + E_{\text{surface}} + E_{\text{volume}} + E_{\text{viscosity}}. \quad (8)$$

A. Diffusion scheme

Since the motion of the fluid particles takes care of advection, we need only to solve the diffusion on the current fluid particles configuration; $\partial C(\vec{x},t)/\partial t = D\boldsymbol{\nabla}^2 C(\vec{x},t)$, where we have assumed that the diffusion constant D is constant and isotropic. Including an anisotropic or spatially varying D is a trivial extension of our method. We assume that the fluid particles carry chemical morphogens, whose distribution is uniform over a given fluid particle. Equivalently we can associate the chemical concentration with the center of mass of the particles and think of the diffusion as taking place between them (a FE view). Because the shape and volume of the fluid particles are irregular, their centers of mass do not correspond to lattice points. We then need a numerical scheme for diffusion among fluid particles. Few existing algorithms solve diffusion on a random or irregular lattice. The more sophisticated and accurate ones are computationally expensive [36]. We use a naive iterated Euler method, which is fast and stable and reproduces different biological experiments with good qualitative and fair quantitative accuracy. We could of course, use a more elaborate scheme, if necessary. We locally average the concentration among the particle's nearest neighbors. The particle neighbors change as the fluid flows. We approximate the Laplacian $\boldsymbol{\nabla}^2 C(\vec{\mathbf{r}},t)$ [where $C(\vec{\mathbf{r}},t)$ is the chemical concentration and $\vec{\mathbf{r}}$ is the center of mass coordinate of a fluid particle] by [39]

$$D\boldsymbol{\nabla}^2 C_j(t) \sim D \sum_{i \text{ next to } j} \frac{[C_i(\vec{\mathbf{r}},t) - C_j(\vec{\mathbf{r}},t)]}{R^2}, \quad (9)$$

where R is the average radius of the fluid particles assuming them to be spherical $[R = (\Sigma_{i=1}^{N} V_i^{1/3})/N]$, and $C_i(\vec{\mathbf{r}},t)$ is the concentration in nearest neighbor fluid particles. We use R^2 instead of $|\vec{\mathbf{r}}_i - \vec{\mathbf{r}}_j|^2$ to avoid Neumann instability. We can update the concentration once or multiple times per MCS depending on the diffusion coefficient of the chemical morphogen. D along with the number of concentration updates per MCS controls the diffusion constant. For larger diffusion coefficients we update the diffusion step multiple times per MCS. For typical chemical morphogens like cAMP the diffusion constants are $\sim 10^{-4}$ μm^2/s, corresponding to a spread of $3\sqrt{2.\times 10^{-4}}$ μm(0.04 μm) per MCS. The typical lattice spacing in our CPM corresponds to 0.1–1.0 μm, hence a fluid particle has a width of $\sim$0.3–3.0 μm. Therefore a very small amount of chemical needs to diffuse among adjacent fluid particle per MCS. In fact, for most practical purposes we need at most one diffusion step per five to ten MCS. Both reflecting and constant concentration (zero concentration is absorbing) boundaries are simple to implement. For reflecting boundary condition we exclude from the exchange of concentration [Eq. (9)] any particle whose boundary is reflecting. For absorbing boundary condition (constant concentration), we define the particles whose boundaries are absorbing to always have zero concentration. The algorithm handles moving boundaries automatically and conserves chemical concentration, unlike many other methods.

III. RESULTS AND DISCUSSION

A. Poiseuille flow

We first discuss simulating Poiseuille flow of a viscous fluid in a cylindrical tube with rigid walls under a uniform

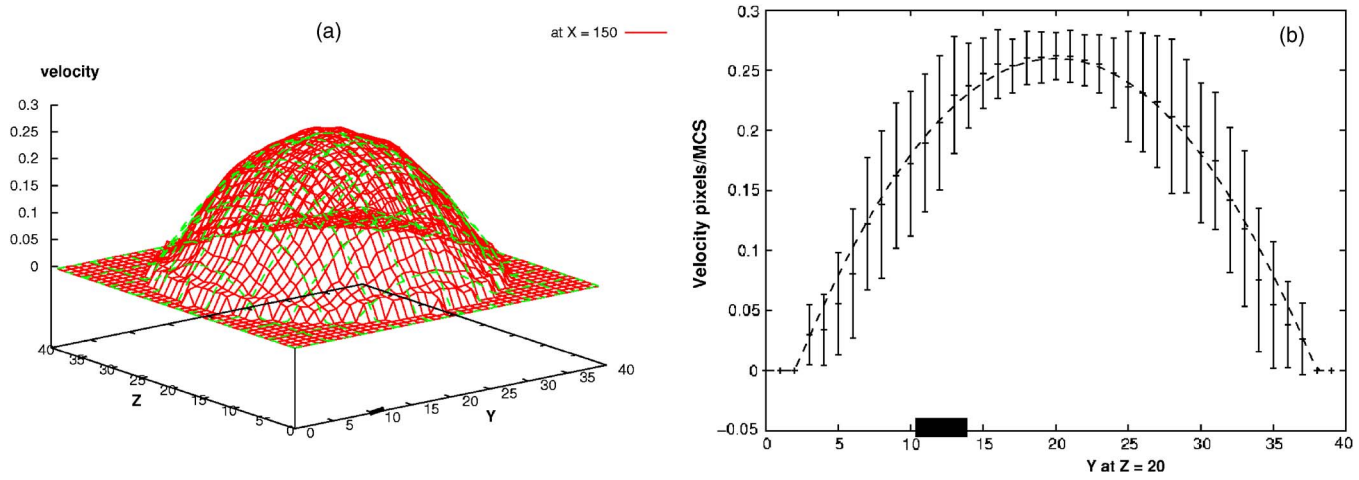

FIG. 2. (Color online) (a) Velocity profile in a cylindrical flow under gravity and its fit to the analytical solution. (b) Velocity profile across a diameter of the tube with error bars, the bold segment along the $\hat{x}$ direction denotes the width of a fluid particle.

force field (body force) using the CPM. We consider a cylindrical tube with a circular cross section of radius 18 lattice units and length 200 lattice units with periodic boundary condition along the length. Each fluid particle has an average volume of 64 lattice points. Our CPM AD scheme works for small forces when the fluid particles remain simply connected. Figure 2 plots the ensemble averaged (50 different initial configurations) cross-sectional profile of the viscous flow at $x=150$ and $t=2000$ MCS with a small force $\vec{F}=0.05\hat{x}$ applied on all the fluid particles. The flow is in the x direction only.

The profile is parabolic as expected. We also show its fit to the analytical solution $V(r)=F/4\eta R^2[1-(r/R)^2]$, where η is the viscosity (a fitting parameter), $R=18$ is the radius of the cylinder, and r is the distance from the axis of the cylinder. What is surprising is the excellent agreement (an error of $<5\%$ with the analytical result despite the coarseness) of the simulation (only 9 particles across the diameter). All lattice points inside a fluid particle have the same velocity, so regions where the shapes of the fluid particles are regular for most ensembles will produce plateaux in the velocity profile. Since in the CPM, the velocity of fluid particles is the center of mass velocity, a lattice point touching a boundary wall will have a small nonzero velocity as the center of mass of the corresponding particle lies in the interior (slip boundary). Since the energy contribution of the constraints near a boundary wall dominates the external applied force and the Monte Carlo temperature, boundary particles are more regular in shape than interior particles. This regularity holds in all ensembles, hence the rms error in the velocity near a boundary wall is small as shown in Fig. 3(b) and the velocity just near the boundary in Fig. 2 has a small plateau. Reducing the size of the fluid particles compared to the typical length scales of the flow reduces these anomalies. Increasing $\lambda_{\text{viscosity}}$ increases the viscosity coefficient η. A future paper will study the relation between η and λ, Monte Carlo temperature, fluid particle size, etc. We shall also show additional biologically relevant hydrodynamic flows.

We next verify our diffusion scheme under various biologically relevant conditions. CPM models using the modified finite temperature Metropolis algorithm have diffusion due to the movement of the CPM cells themselves which adds to the diffusion of chemical morphogens. However for most CPM simulations, e.g., a temperature 0.1 and other parameter values used throughout this paper, the diffusion coefficient of the CPM cells is $\sim 10^{-4}$ pixel^2/MCS, which is much smaller than the typical diffusion coefficient of ~ 0.1 that we treat in this paper. Hence for pure diffusion in a static medium the fluid is effectively fixed. Besides the concentra-

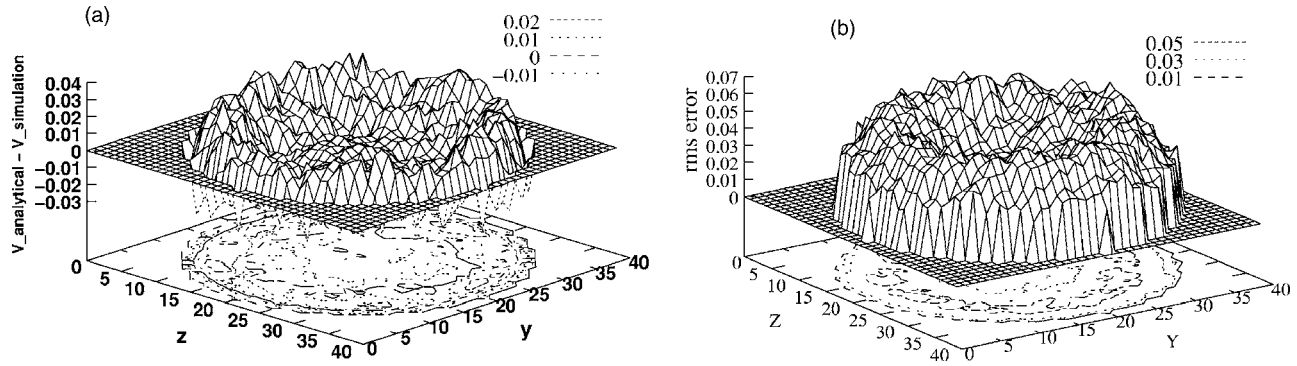

FIG. 3. (a) The absolute error between the analytical solution $V_{\text{analytical}}$ and the CPM simulation $V_{\text{simulation}}$ at $x=150$. (b) The rms error of over 50 ensembles.

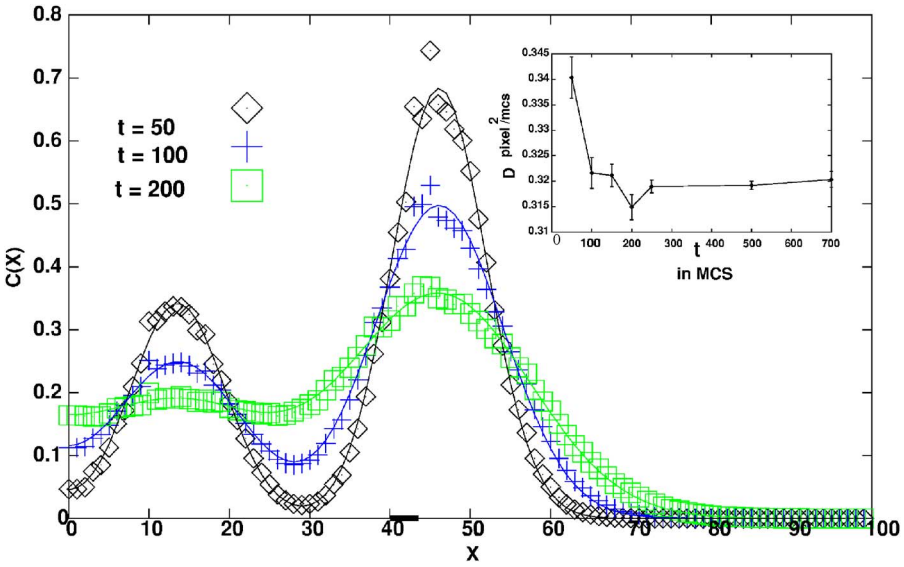

FIG. 4. (Color online) Symbols denote chemical profile projected on the x axis (summing in the Y and Z directions) at $t=50$, 100, and 200 MCS for reflecting barriers at $x=0$ and 100 denoted by symbols. The solid line is a fit to the exact solution using the fitting parameter D. The inset shows variations in D with time, due to coarse graining and the initial sharp distribution.

tion profile of the diffusing chemical in a medium, diffusion in the presence of boundaries, and moving source is crucially important in biology. We show that the results of our simple CPM diffusion from CPM agree very well with corresponding analytical calculations or finite element results. We also briefly discuss the validity of our method for diffusion in Poiseuille flow.

The four cases we discuss below employ fluid particles with a target volume $v_{\text{target}}=27$, unless we mention otherwise. The lattice has $100\times100\times100$ sites. We equilibrate and quench to remove any disconnected cells which the finite-temperature equilibration produces [27]. In our model a chemical source at a given lattice point gives all lattice points which belong to the fluid particle containing that chosen point the same concentration. We apply one diffusion step per MCS. The first three cases are for static fluids.

B. Two sources with reflecting and absorbing boundaries

We consider two point sources at 15, 50, 50 and 50, 50, 50 with initial concentrations (at $t=0$) of 5 and 10, respectively. The chemicals diffuse from these instantaneous sources. The bounding planes of the cube are reflecting. Figure 4 plots the corresponding one-dimensional diffusion profile projection (with no ensemble average) after elapsed times $t=50$, 100, 200 MCS, and fitted to the exact solution

$$C(x,t) = 10.0/\sqrt{(4\pi Dt)}(\exp^{[-(x-x1)^2]/4Dt} + \exp^{[-(2L1-x-x1)^2]/4Dt} + \exp^{[-(2L2-x-x1)^2]/4Dt}) + 5.0/\sqrt{(4\pi Dt)}(\exp^{[-(x-x2)^2]/4Dt} + \exp^{[-(2L1-x-x2)^2]/4Dt} + \exp^{[-(2L2-x-x2)^2]/4Dt}),$$

D being a fit parameter. Here $L1$ and $L2$ are the coordinates of the two reflecting boundaries and $x1$ and $x2$ are the coordinates of the instantaneous sources. The diffusion profile matches very well at all times, even near the boundaries. The maximum relative error (compared to the exact solution) at $t=50$ MCS is 5%, again, surprisingly good for such a coarse simulation. We discuss errors in detail for absorbing boundary conditions in the next paragraph. The inset shows the variation of the diffusion coefficient calculated from fitting to

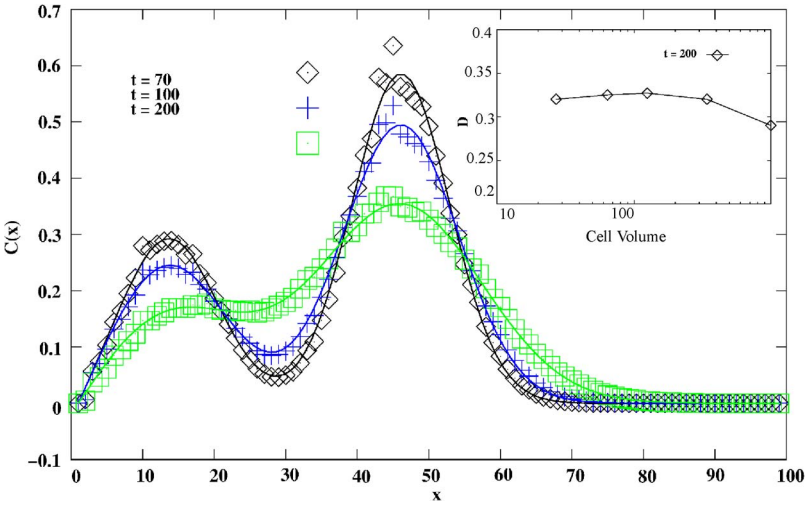

FIG. 5. (Color online) Chemical profile projected on the x axis from diffusion of two instantaneous point sources for an absorbing barrier at $x=0$ and $x=100$ for $t=70$, 100, and 200 MCS. The inset shows the variation of D with fluid particle volume on a log scale.

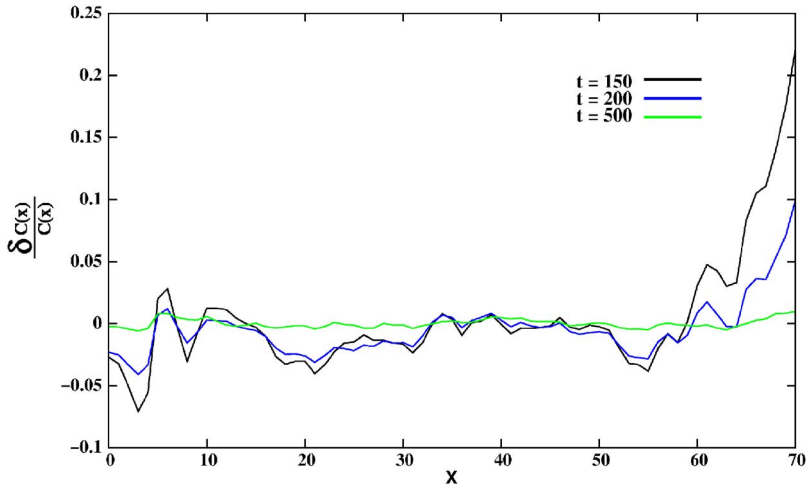

FIG. 6. (Color online) Relative error along the x lattice direction for an absorbing barrier.

the exact solution as a function of time. Though the diffusion constant should remain constant with time, we observe a 5–6 % variation from the asymptotic value at *small times* due to the sharp initial distribution producing structures smaller than the fluid particle scale of our coarse-grained scheme. We also studied the variation of the diffusion coefficient D as a function of the target volume of the fluid particles. D is constant for variations over one order of magnitude of the

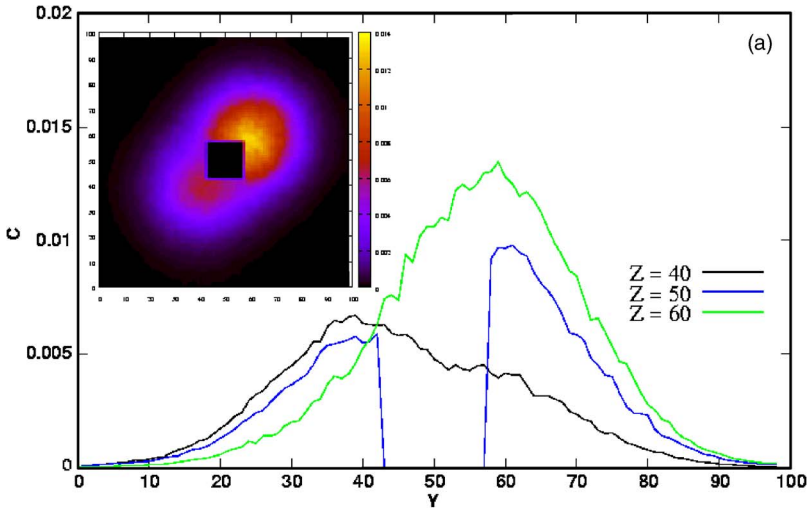

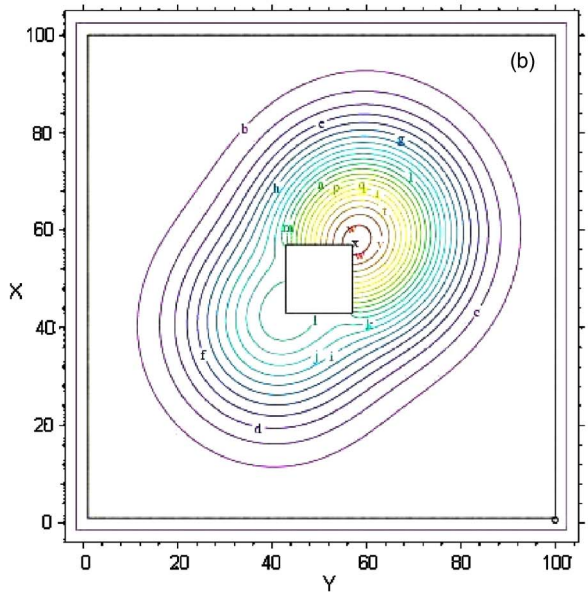

FIG. 7. (Color online) Chemical profile cross section along z=40, 50, and 60 in the presence of a cylindrical reflecting barrier with axis along the $\hat{x}$ direction and rectangular cross section. The sources with initial concentration 5 and 10 are placed at 50, 40, 40 and 50, 60, 60. The inset shows 2D projection of the profile. The lower figure shows a two-dimensional projection obtained from finite element calculations. The concentration decreases as we go away from the center contours (yellow lines).

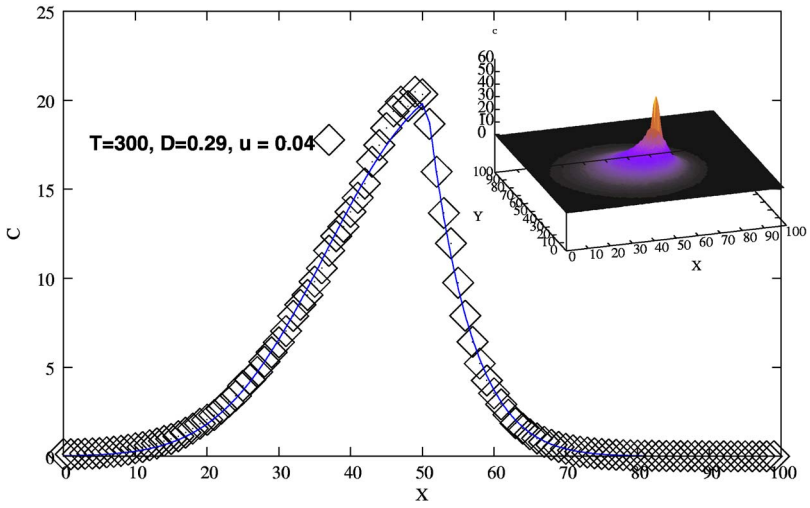

FIG. 8. (Color online) CPM simulation of the chemical profile from a moving source (the other two coordinates integrated out) at $t=300$ MCS. The solid line denotes the fit to Eq. (10). The inset shows a two-dimensional projection of the simulation, where red denotes the highest chemical concentration and black the lowest.

target volume of the fluid particles as shown in the inset to Fig. 5. Figure 5 also shows the chemical profile for an absorbing barrier at $x=0$ and $x=100$. The figures show that the diffusion coefficient for both reflecting and absorbing barriers cases is same. Hence for a wide range of fluid particle volumes, our CPM ADE algorithm faithfully reproduces diffusion from two point sources.

Figure 6 plots the relative error as a function of position at different times. As mentioned in the last paragraph the sharp distribution at the initial time produce errors large compared to later time, i.e., if we ignore the large errors in the tail (as the magnitude of concentration is extremely small in the tails) the relative error at $t=150$ is $<5\%$ whereas at $t=500$ it is $<0.5\%$. In the actual biological situation, cells secrete chemical morphogens over their whole membrane surface and hence such singular cases of high point concentration of chemical rarely occur.

C. Two sources with a reflecting obstacle inside the medium

Since biological cells can be impermeable to many chemical morphogens, they can act as reflecting boundaries within the fluid medium. We check this situation for the simple test case of a cylindrical barrier with rectangular cross section [15×15, pixels centered at (50, 50, 50) and the axis along the x direction] within the fluid medium. As in the previous case, we place two point sources near the two opposite corners of the rectangle at (50, 40, 40) and (50, 60, 60).

We recover the same diffusion coefficient as in the previous case. Figure 7 plots the one-dimensional cross section of the diffusion profile at three different z positions. Along $z=40$ and 60 the barrier is absent and the diffusion is merely the superposition of that from the two sources. Along $z=50$ we see the effect of the reflecting barrier. The inset on the right side shows the concentration profile obtained from a finite element calculation for this situation which matches very well with the CPM concentration profile in the left inset.

D. Moving continuous source

Moving cells often secrete morphogens. Hence we correctly simulate cells' chemotactic response to secreted chemicals only if we faithfully reproduce diffusion from moving sources. To test our simulation we assign an arbitrary fluid particle a constant concentration C_0 (continuous source) and uniform velocity v along the x direction. We keep the source sufficiently distant from the boundary to avoid bound-

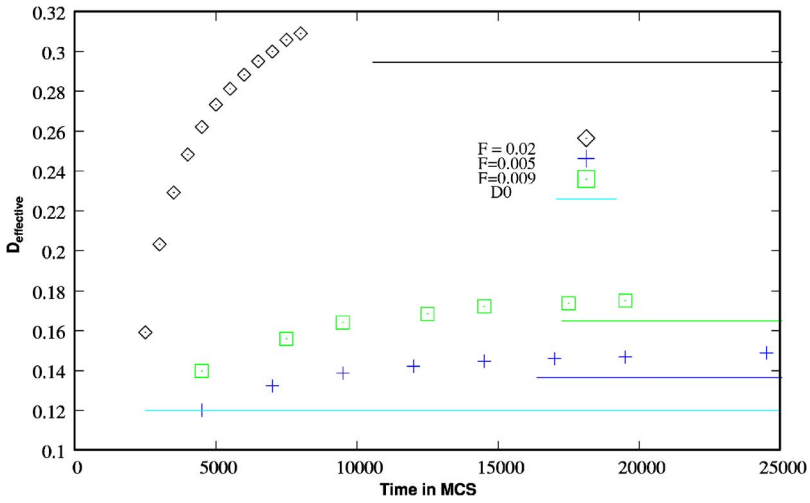

FIG. 9. (Color online) Effective diffusion coefficient for mean flow velocities $\bar{v}=0.056$, 0.028, and 0.016, respectively from top to the bottom curve. The solid lines show the analytical results corresponding to above mean velocities.

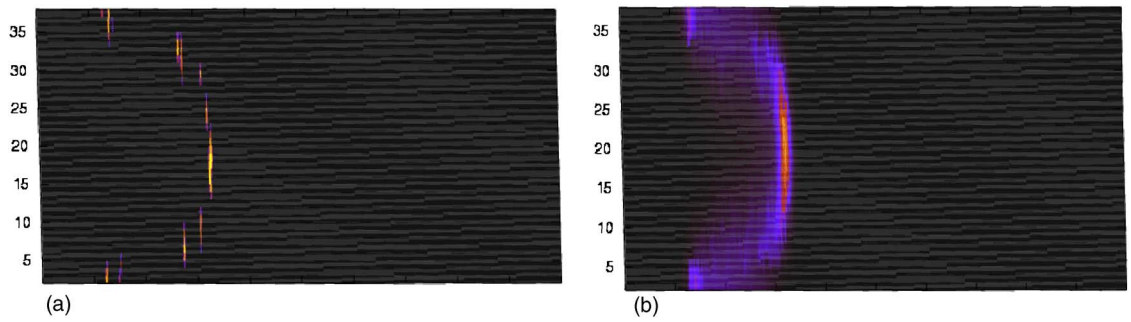

FIG. 10. (Color online) Cross-sectional profile ($\hat{x}$-$\hat{z}$ plane, $y=20$) of chemical concentration at $t=500$ MCS starting from an initial set of particles at $x=75$ with uniform concentration; (a) with no diffusion, (b) with diffusion. Particles which move away from the plane in the $\hat{y}$ direction cannot be seen in the figures.

ary effects. At $t=0$ the source is at $x=35$ and moves with velocity $u=0.04$ pixel/MCS. We fit the CPM chemical profile projection in the x direction (no ensemble average) with the 1D analytical solution

$$\alpha(x) = [(x - x_0)^2]/(4D), \tag{10}$$

$$\beta = u^2/(4D), \tag{11}$$

$$\gamma(x) = \exp[(x - x_0)u/(2D)], \tag{12}$$

$$C(x,t) = \frac{C_0}{2}\gamma(x)[\exp(2\sqrt{\alpha(x)\beta}\,]\mathrm{Erfc}\left(\sqrt{\frac{\alpha(x)}{t}} + \sqrt{\beta t}\right) \tag{13}$$

$$+ \exp[-2\sqrt{\alpha(x)\beta}]\mathrm{Erfc}\left(\sqrt{\frac{\alpha(x)}{t}} - \sqrt{\beta t}\right). \tag{14}$$

Figure 8 shows that the CPM diffusion agrees very well with the analytical solution. The diffusion coefficient obtained from the fit is $D=0.29$.

E. Taylor-Aris dispersion in Poiseuille flow

We check the qualitative agreement of the dispersion coefficient obtained using our CPM ADE solver for Poiseuille flow along the x direction (described in Sec. III A) in a cylindrical geometry. We compare our result for an initial delta distribution of chemical in the middle of the tube. After an initial transient, so that the chemical reaches the boundary in the y and z directions, we compare the diffusion coefficient of chemical distribution along the x direction with the analytical result for the effective diffusion coefficient in Poiseuille flow along the cylinder axis, i.e., $D_{\text{effective}}=D_0 + \bar{v}^2R^2/48D_0$. Here D_0 is the diffusion coefficient in the absence of flow, $\bar{v}$ is the average velocity, and R is the radius of the cylinder. Figure 9 shows our results where we have plotted the variation of effective diffusion coefficient with time (in MCS) for different mean velocities. For the analytical results given in solid lines in Fig. 9, we use the mean velocity obtained from the fit of the velocity profile as shown in Fig. 2. Figure 10 shows snapshots of chemical profile after 500 MCS for $D_0=0$ and $D_0=0.12$. In this case, we start with a thin sheet of chemical in the x-z plane, at $x=75$, i.e., all the particles at $x=75$ have uniform concentration. We take a cut at $y=20$ to see the evolved chemical profile. A detailed study of evolution of chemical profile, effect of embedded objects like sphere under both stationary and moving conditions will be reported in our future communication.

IV. CONCLUSIONS

We have implemented fluid flow, advection, and diffusion in the framework of the CPM, avoiding the programming complexity and computational demands associated with implementing a finite-element or finite-difference Navier-Stokes simulation and interfacing it with the CPM lattice.

We have used three biologically relevant test cases to verify our method. All our results for diffusion in the presence of boundaries or moving sources agree very well with corresponding analytical or finite-element solutions. The errors in our scheme are large if we try to probe far below the diffusion time scale or the fluid particle length scale, but the results are qualitatively correct. Thus we must be cautious when applying this scheme to large Pe number flows. The requirement that fluid particles remains connected, limits the method to low Re. However, since most biological mechanisms operate at low Re our CPM ADE solver is appropriate for many cell-level simulations.

[1] C. R. Nugent, W. M. Quarles, and T. H. Solomon, Phys. Rev. Lett. **93**, 218301 (2004); J. D. Seymour, J. P. Gage, S. L. Codd, and R. Gerlach, *ibid.* **93**, 198103 (2004); M. Leconte, J. Martin, N. Rakotomalala, and D. Salin, *ibid.* **90**, 128302 (2003); B. F. Edwards, *ibid.* **89**, 104501 (2002).

[2] A. Bancaud, G. Wagner, K. D. Dorfman, and J. L. Viovy Anal. Biochem. **77**, 833 (2005).

[3] T. Yanagita and K. Kaneko, Phys. Rev. Lett. **78**, 4297 (1997).

[4] J. M. Keller and M. L. Brusseau, Environ. Sci. Technol. **37**, 3141 (2003); T. E. McKone and D. H. Bennett, *ibid.* **37**, 3123 (2003).
[5] G. J. Gibson, C. A. Gilligan, and A. Kleczkowski, Proc. R. Soc. London, Ser. B **266**, 1743 (1999); J. T. Truscott and C. A. Gilligan, Proc. Natl. Acad. Sci. U.S.A. **100**, 9067 (2003).
[6] T. E. Faber, *Fluid Dynamics for Physicists* (Cambridge University Press, Cambridge, England, 1995).
[7] P. M. Gresho and R. L. Sani, *Incompressible Flow and the Finite Element Method* (Wiley, New York, 2000); W. Hundsdorfer and J. G. Verwer, *Numerical Solution of Time-Dependent Advection-Diffusion-Reaction Equations*, Springer Series in Computational Mathematics (Springer, New York, 2003).
[8] Y. H. Qian, D. D'Humieres, and P. Lallemand, Europhys. Lett. **17**, 479 (1992).
[9] E. G. Flekkoy, Phys. Rev. E **47**, 4247 (1993).
[10] S. P. Dawson, S. Chen, and G. D. Doolean, J. Chem. Phys. **98**, 1514 (1993).
[11] C. P. Lowe and D. Frenkel, Physica A **220**, 251 (1995); R. H. Merks *et al.*, J. Comput. Phys. **183**, 563 (2002).
[12] J. C. Anthony, J. Fluid Mech. **271**, 285 (1994).
[13] W. Zeng, G. L. Thomas, S. A. Newman, and J. A. Glazier, *Mathematical Modeling and Computing in Biology and Medicine, 5th ESMTB Conference 2002*, edited by V. Capasso (Societ Editrice Esculapio, Bologna, 2003).
[14] A. M. Turing, Philos. Trans. R. Soc. London, Ser. B **237**, 266 (1952); A. Taylor, Prog. React. Kinet. **27**, 247 (2002).
[15] D. V. Zhelev, A. M. Alteraifi, and D. Chodniewicz, Biophys. J. **87**, 688–695 (2004).
[16] H. C. Berg and P. M. Tedesco, Proc. Natl. Acad. Sci. U.S.A. **72**, 3235 (1975).
[17] M. H. Kroll, J. D. Hellums, L. V. McIntire, A. L. Schafer, and J. L. Moake, Blood **88**, 1525 (1996).
[18] S. Jadhav and K. Konstantopoulos, Am. J. Physiol.: Cell Physiol. **283**, C1133 (2002).
[19] M. U. Nollert, N. J. Panaro, and L. V. McIntire, Ann. N.Y. Acad. Sci. **665**, 94 (1992); P. F. Davies, Physiol. Rev. **75**, 519 (1995).
[20] E. B. Finger, K. D. Puri, R. Alon, M. B. Lawrence, U. H. von Andrian, and T. A. Springer, Nature (London) **379**, 266 (1996).
[21] A. D. Taylor, S. Neelamegham, J. D. Hellums, C. W. Smith, and S. I. Simon, Biophys. J. **71**, 3488 (2004).
[22] M. Pavlin, N. Pavselj, and D. Miklavcic, IEEE Trans. Biomed. Eng. **49**, 605 (2002).
[23] H. G. E. Hentschel, J. A. Glazier, and S. A. Newman, Proc. R. Soc. London, Ser. B **271**, 1713 (2004).
[24] S. Kikichi *et al.*, Neural Networks **16**, 1389 (2003).
[25] M. S. Alber, A. Kiskowski, J. A. Glazier, and Y. Jiang, Math. Syst. Theory Biology, Communication, and Finance **134**, 1 (2003).
[26] F. Graner and J. A. Glazier, Phys. Rev. Lett. **69**, 2013 (1992).
[27] J. A. Glazier and F. Graner, Phys. Rev. E **47**, 2128 (1993).
[28] W. Zeng, G. L. Thomas, and J. A. Glazier, Physica A **341**, 482 (2004).
[29] M. Zajac, G. L. Jones, and J. A. Glazier, Phys. Rev. Lett. **85**, 2022 (2000).
[30] S. Maree, Ph.D. thesis University Utrecht, 2000; A. F. MarAee and P. Hogeweg, Proc. Natl. Acad. Sci. U.S.A. **98**, 3879 (2001).
[31] Emma Stott, N. F. Britton, J. A. Glazier, and M. Zajac, Math. Comput. Modell. **30**, 183 (1999).
[32] R. M. H. Merks, S. A. Newman, and J. A. Glazier, Lect. Notes Comput. Sci. **3305**, 425 (2004).
[33] R. Chaturvedi, J. A. Izaguirre, C. Huang, T. Cickovski, P. Virtue, G. Thomas, G. Forgacs, M. Alber, G. Hentschel, S. A. Newman, and J. A. Glazier, Lect. Notes Comput. Sci. **2659**, 39 (2003).
[34] Y. Jiang, *Cellular Pattern Formation*, Ph.D. dissertation, University of Notre Dame, 1998.
[35] E. M. Purcell, Am. J. Phys. **45**, 3 (1977).
[36] J. Braun and M. Sambridge, Nature (London) **376**, 655 (1995).
[37] M. E. J. Newman and G. T. Barkema, *Monte Carlo Methods in Statistical Physics* (Oxford University, New York, 1999).
[38] S. Wong, Ph.D. thesis, Notre Dame University, 2004.
[39] J. D. Murray, *Mathematical Biology*, Vol. 1 (Springer-Verlag, Berlin, 2002).
[40] E. M. Lifsihtz and L. D. Landau, *Fluid Mechanics* (Butterworth-Heinemann, Oxford, 1987).